High temperature oxidation of iridium
by Steven Wayne Hills

A thesis submitted in partial fulfillment of the requirements of the degree of MASTER OF SCIENCE in Mechanical Engineering
Montana State University

Abstract:
An investigation of the oxidation of heated iridium wires was performed in the temperature range of 1675 to 2260°C (1948 to 2533°K). The wires were oxidized in naturally convected oxygen and air in the pressure range of 9.8 x 10-8 to 1.32 atmospheres (7.5 x 10-5 to 1000 torr) and in force-convected oxygen and air at pressure from 0.0046 to 1.32 atmospheres (3.5 to 1000 torr). The experimental results were compared to values calculated by a theoretical equation whose development was based on control of the oxidation by the rates of evaporation of Ir(g), Ir03(g), and IrO3(g) and by the rates of the subsequent diffusion of these species through the gaseous boundary layer.

Empirical equations were developed which describe the temperature dependencies of the standard-state free-energies of formation of IrO2(g) and IrO3(g). An equation was developed for the Nusselt number for natural-convection heat transfer from the high temperature wires. Also, an earlier equation for the thermal expansion of iridium was revised.

STATEMENT OF PERMISSION TO COPY

In presenting this thesis in partial fulfillment of the requirements for degree of Master of Science in Mechanical Engineering at Montana State University, I agree that the Library shall make it freely available for inspection. I further agree that permission for extensive copying of this thesis for scholarly purposes may be granted by my major professor, or, in his absence, by the Director of Libraries. It is understood that any copying or publication of this thesis for financial gain shall not be allowed without my written permission.

Signature Steven Wayne Hills

Date Dec. 9, 1974

HIGH TEMPERATURE OXIDATION OF IRIDIUM

by

Steven Wayne Hills

A thesis submitted in partial
fulfillment of the requirements of the degree

of

MASTER OF SCIENCE

in

Mechanical Engineering

Approved:

Harry W. Torrus
Chairman, Examining Committee

Dennis O. Blackketter
Head, Major Department

[signature]
Graduate Dean

MONTANA STATE UNIVERSITY
Bozeman, Montana

December, 1974

ACKNOWLEDGMENTS

Special thanks and appreciation are extended to Dr. R.T. Wimber for his guidance and assistance in the development of this research project. Dr. H.W. Townes, Dr. D.O. Blackketter, and Dr. J.A. Scanlan are also thanked for serving on the thesis committee.

A special word of thanks is also due my wife JoAnne for her effort in typing this thesis.

TABLE OF CONTENTS

	Page
VITA	ii
ACKNOWLEDGMENTS	iii
LIST OF TABLES	vi
LIST OF FIGURES	vii
ABSTRACT	viii
CHAPTER I. INTRODUCTION	
Characteristics and Uses of Iridium	1
Review of Previous Work	2
CHAPTER II. THEORETICAL CONSIDERATIONS	
Oxidation Characteristics of Solid Materials	5
Theoretical Model for the Oxidation of Iridium	6
CHAPTER III. EXPERIMENTAL PROCEDURES FOR NATURAL CONVECTION REGIME	
Experimental Materials	14
Apparatus and Procedure	14
CHAPTER IV. RESULTS AND DISCUSSION OF NATURAL-CONVECTION OXIDATION	
Experimental Data	20
Calculation of Theoretical Rates	22
CHAPTER V. EXPERIMENTAL PROCEDURES FOR FORCED CONVECTION REGIME	
Experimental Materials	38
Apparatus and Procedure	38
CHAPTER VI. RESULTS AND DISCUSSION OF FORCED CONVECTION OXIDATION	
Experimental Data	42
Calculation of Theoretical Rates	44

CHAPTER VII. SUMMARY 50

APPENDIX A 52

APPENDIX B 59

REFERENCES 62

LIST OF TABLES

Page

TABLE 1 - Average Deviation of Theoretical Equation from Experimental Data for Naturally Convected Oxidation in Pure Oxygen 25

TABLE 2 - Average Deviation of Theoretical Equation from Experimental Data for Naturally Convected Oxidation in Air 25

TABLE 3 - Properties of Oxygen 31

TABLE 4 - Properties of Air 32

TABLE 5 - Average Deviation of Theoretical Equation from Experimental Data for Force-Convected Oxidation at Low Reynolds Numbers in Pure Oxygen 43

TABLE 6 - Experimental Data for Naturally Convected Oxidation in Pure Oxygen 53

TABLE 7 - Experimental Data for Naturally Convected Oxidation in Air 57

TABLE 8 - Experimental Data for Force-Convected Oxidation at Low Reynolds Numbers in Pure Oxygen 60

TABLE 9 - Experimental Data for Force-Convected Oxidation at High Reynolds Numbers 61

LIST OF FIGURES

Page

Figure 1 - Schematic Representation of Natural-Convection Oxidation Apparatus 16

Figure 2 - Example of a Rate Plot from a Typical Oxidation Experiment 21

Figure 3 - Experimental Results and Theoretical Correlation for Naturally Convected Oxidation in Pure Oxygen . . 23

Figure 4 - Experimental Results and Theoretical Correlation for Naturally Convected Oxidation in Air 24

Figure 5 - Resultant Free Energies of Formation 35

ABSTRACT

An investigation of the oxidation of heated iridium wires was performed in the temperature range of 1675 to 2260°C (1948 to 2533°K). The wires were oxidized in naturally convected oxygen and air in the pressure range of 9.8×10^{-8} to 1.32 atmospheres (7.5×10^{-5} to 1000 torr) and in force-convected oxygen and air at pressure from 0.0046 to 1.32 atmospheres (3.5 to 1000 torr). The experimental results were compared to values calculated by a theoretical equation whose development was based on control of the oxidation by the rates of evaporation of Ir(g), $IrO_2(g)$, and $IrO_3(g)$ and by the rates of the subsequent diffusion of these species through the gaseous boundary layer.

Empirical equations were developed which describe the temperature dependencies of the standard-state free-energies of formation of $IrO_2(g)$ and $IrO_3(g)$. An equation was developed for the Nusselt number for natural-convection heat transfer from the high temperature wires. Also, an earlier equation for the thermal expansion of iridium was revised.

CHAPTER I

INTRODUCTION

Characteristics and Uses of Iridium

An oxidation study of iridium is of engineering interest because it is the only elemental metal known to man that has a high enough melting point (2454°C or 2727°K) and a low enough oxidation rate that it can survive for extended periods of time at temperatures greater than 2000°C in an oxygen bearing atmosphere. In fact, iridium is one of the most corrosion resistant metals known when it is compared to other metals as they are subjected to a wide variety of environments at high temperatures. Iridium is quite resistant to corrosive attack by acids, salt solutions, fused salts, molten metals, and molten metal oxides.

A general oxidation characteristic of iridium is that a thin oxide film is formed on the surface when the metal is subjected to temperatures in the range of 600 to 1000°C in the presence of oxygen. However, at temperatures greater than 1000°C volatile oxides are formed and the surface of the metal is left clean and shiny. It is this formation of volatile oxides which causes the oxidation rate to become linear with respect to time at the higher temperatures.

Iridium is presently available in commercial quantities as iridium and iridium-rhodium alloy wires which are used as standardized high temperature thermocouples and filaments in high temperature electric

furnaces. Other uses of iridium as a structural material are limited even though its strength properties at high temperature are quite desirable. The principal drawback of using iridium is the cost. Being a platinum group metal, iridium is very expensive. Another limitation of using iridium as a structural material is the weight factor. At 22.57 gm/cm^3, iridium is one of the most dense elements known to man. Thus, the most promising use of iridium appears to be in the form of coatings to protect structural materials from rapid oxidation at high temperatures.

Potential applications for iridium coatings are nuclear reactor components, assemblies in rocket and gas turbine engines, leading edges of re-entry spacecraft, and other applications where oxygen exposed surfaces are subjected to high temperature. The very low emittance of iridium could restrict its use on spacecraft where the ambient pressure is slight and the primary means of heat dissipation is by radiation.

Review of Previous Work

Wimber [1] has made a thorough review of the information available from other experimenters' work. A brief summary of that review is presented here.

The composition of the oxides of iridium and the kinetics of the chemical reactions involved have been investigated by several

independent researchers. Cordefunke and Meyer [2] passed oxygen bearing gas over iridium metal in the temperature range of 1169 to 1462°C (1442 to 1735°K). They concluded that $IrO_3(g)$ was the major compound formed. Cordfunke and Meyer also obtained values of the equilibrium constants that were slightly higher than those noted by Alcock and Hooper [3] and Schafer and Heitland [4]. Holburn, Henning, and Austin [5] studied heated iridium foil exposed to oxygen in gases flowing slowly past the foil. They also concluded that $IrO_3(g)$ was the main oxide formed.

Mass spectrometric studies made by Norman et al [6] caused them to conclude that both $IrO_2(g)$ and $IrO_3(g)$ were formed in appreciable quantities when iridium was oxidized. They also noted that the presence of IrO(g) could not be ruled out but its partial pressure was estimated to be less than 2 percent of the partial pressure of $IrO_2(g)$. In this same study the values for the standard-state enthalpies of formation for $IrO_2(g)$ and $IrO_3(g)$ were reported as 48.5 $\pm$ 0.8 kcal/mole and 5.5 $\pm$ 1.5 kcal/mole, respectively.

Olivei [7] also concluded from his studies that $IrO_2(g)$ and $IrO_3(g)$ were the major oxide species formed. He performed mass spectrometric studies in the range of 627 to 2227°C (900 to 2500°K) which yielded a standard-state enthalpy of formation for $IrO_3(g)$ of 6.0 kcal/mole.

On the basis of this preliminary work recent studies have been made at Montana State University of the surface recession rate of hot oxidizing iridium wires. Wimber and Kraus [8] concluded that Ir(g) was also an important species at high temperature and that IrO(g) contributed very little to the overall recession rate. In this study a theoretical model was derived to predict the surface recession rate of iridium wires in the temperature range of 1675 to 2260°C (1948 to 2533°K) as they were oxidized in pure oxygen at pressures ranging from 1.32×10^{-3} to 1.32 atmospheres (1 to 1000 torr). Wahl [9] extended the experimental data to lower pressures in oxygen (7.5×10^{-6} torr) and also oxidized the wires in air. This study showed that two theoretical models were needed to describe the recession rates; one was used at low pressures and one was used at high pressures.

On the basis of information gathered by these investigators it was proposed that a theoretical model can be developed which will predict the surface recession rate of oxidizing iridium wires over the temperature range of 1675 to 2260°C (1948 to 2533°K) and throughout the pressure range of 9.8×10^{-8} to 1.32 atmospheres (7.5×10^{-5} to 1000 torr) in oxygen or air. Furthermore, it is expected that this model will be valid for wires in both naturally convected and force convected regions.

CHAPTER II

THEORETICAL CONSIDERATIONS

Oxidation Characteristics of Solid Materials

A study of the general corrosion of a material leads to a study of the specific chemical reactions which can occur under the imposed conditons. A consideration of the equilibrium constants of these reactions reveals the most thermodynamically stable point toward which the reactants will tend to move.

From an engineering view point, the most applicable facet of corrosion is a determination of the rate at which it takes place. To find the rate of corrosion the rates of the steps involved in the reaction mechanism must be found or, if one step of the mechanism is much slower than the others, the rate of this "rate controlling step" must be determined.

In the case of a solid oxidizing in a fluid where all of the oxides formed are volatile, the corrosion rate is expected to be controlled by one or more of the following steps of oxidation:

1) Diffusion of the oxygen through the fluid and through the boundary layer next to the surface.
2) Adsorption of the oxygen onto the surface.
3) Reaction of the oxygen with the solid material on the surface.

4) Desorption of the oxide from the surface.

5) Diffusion of the oxide through the boundary layer away from the material.

Theoretical Model for the Oxidation of Iridium

Wimber [10] previously derived a model which takes into account the formation of Ir(g), IrO(g), IrO_2(g), and IrO_3(g) and their partial pressures at the inner surface of the boundary layer. This model assumes that the oxidation rate is controlled by the rate of diffusion of these gaseous species through the boundary layer. Kraus [11] showed that this model did predict the surface recession rates of the iridium wires quite effectively at pressures in the range of 1.32×10^{-3} to 1.32 atmospheres (1 to 1000 torr). Wahl [9] concluded that this model did not predict the experimentally determined rates at low pressures. It was found that another model was needed for pressures of approximately 10^{-4} atmospheres and below. At these low pressures there is essentially no boundary layer present, and a theoretical model was developed by assuming that the rate controlling step is the surface reactions and/or the desorption of the oxide species from the surface.

With this information in mind, it appears that a theoretical model could be developed from which an equation for the oxidation rate could be written which has a pressure dependency such that at the higher

pressure range the diffusion of the oxide species would predominate and at the lower pressure range the vaporization of the oxide species would predominate.

From the information presented in Chapter I it is assumed that the major oxide species of iridium formed are Ir(g), $IrO_2(g)$, and $IrO_3(g)$. Following this assumption, equilibrium conditions at the gas-metal interface can be represented by the following reactions:

$$Ir(c) + O_2(g)_S \xrightarrow{K_2} IrO_2(g)_S \qquad (1)$$

$$Ir(c) + 3/2\ O_2(g)_S \xrightarrow{K_3} IrO_3(g)_S \qquad (2)$$

$$Ir(c) \longrightarrow Ir(g)_S \qquad (3)$$

where the subscript S denotes conditions at the solid boundary.

Equations (1), (2), and (3) are overall reactions for the process. When the oxygen is adsorbed onto the metal surface it comes in contact with an iridium atom and creates a site for a potential reaction and, following the reaction, a potential desorption or evaporation site of the oxide species. Thus, assuming equilibrium between the oxygen and the metal surface, the following reaction equations can be written:

$$|S_2 \underset{k_{2b}}{\overset{k_{2f}}{\rightleftharpoons}} IrO_2(g)_S \tag{4}$$

$$|S_3 \underset{k_{3b}}{\overset{k_{3f}}{\rightleftharpoons}} IrO_3(g)_S \tag{5}$$

$$|S_M \underset{k_{Mb}}{\overset{k_{Mf}}{\rightleftharpoons}} Ir(g)_S \tag{6}$$

where $|S_2$, $|S_3$, and $|S_M$ are the entities at the sites where the respective vapor species may form and the subscript S denotes a location at the inner surface of the boundary layer. Referring to the reaction represented by Eq. (4), the contribution of the formation of $IrO_2(g)$ to the overall oxidation rate may be expressed as

$$\dot{X}_{S2} = A(k_{2f}C_{S2} - k_{2b}P_{2S}). \tag{7}$$

In Eq. (7) the subscripts 2 refer to quantities pertaining to $IrO_2(g)$ and $\dot{X}$ is a surface recession rate with units of length per time. Also, P_{2S} is the partial pressure of $IrO_2(g)$ at the inner surface of the boundary layer, C_{S2} is the concentration of the $|S_2$ entity, A is an equivalent weight (having the units of mass of iridium consumed per mole of oxide species formed) divided by the density of iridium, and k_{2f} and k_{2b} are the specific reaction rate constants for the reaction of Eq. (4) in the forward and reverse directions, respectively.

A relationship between k_{2f} and k_{2b} which is valid under nonequilibrium conditions may be obtained by considering two different reactions proceeding under equilibrium conditions. The expression involving the equilibrium constant for the overall reaction represented by Eq. (1) is

$$P_2 = K_2 P_{O_2} \tag{8}$$

where P_2 is the partial pressure of $IrO_2(g)$ for an oxygen partial pressure of P_{O_2} and K_2 is the equilibrium constant for the reaction of Eq. (1). Here it should be noted that $P_2 > P_{2S}$. However, at equilibrium conditions no net corrosion is taking place and $P_2 = P_{2S}$. Also the forward reaction rate equals the backward reaction rate at equilibrium. Therefore

$$k_{2f} C_{S2} = k_{2b} P_{2S} = k_{2b} P_2. \tag{9}$$

Substituting Eq. (8) into Eq. (9) gives

$$k_{2f} C_{S2} = k_{2b} K_2 P_{O_2}, \tag{10}$$

or

$$k_{2b} = k_{2f} C_{S2} / (K_2 P_{O_2}). \tag{11}$$

Substitution of Eq. (11) into Eq. (7) gives

$$\dot{X}_{S2} = Ak_{2f}C_{S2}[1 - P_{2S}/(K_2P_{O_2})]. \qquad (12)$$

The vaporization flux can be calculated by the Knudsen modification of the Hertz-Langmuir equation [12]. The flux in moles of vapor molecules that leave the surface per unit area per time is given by

$$J = \alpha_v P_{eq}(2\pi MRT_k)^{-1/2} \qquad (13)$$

where α_v is the vaporization coefficient, P_{eq} is the equilibrium partial pressure of the species, M is the molecular weight of the species, R is the ideal gas constant, and T_k is the absolute temperature of the solid. If only the forward reaction process of Eq. (4) is considered (i.e. evaporation process into a perfect vacuum) the forward rate is equal to the evaporation or $k_{2f}C_{S2} = J_2$ where

$$J_2 = P_2(2\pi M_2RT_k)^{-1/2} = K_2P_{O_2}(2\pi M_2RT_k)^{-1/2} \qquad (14)$$

when α_v is assigned a value of unity.

Thus,

$$k_{2f}C_{S2} = K_2P_{O_2}(2\pi M_2RT_k)^{-1/2}. \qquad (15)$$

Substitution of Eq. (15) into Eq. (12) yields

$$\dot{X}_{S2} = AK_2P_{O_2}(2\pi M_2RT_k)^{-1/2}[1 - P_{2S}/(K_2P_{O_2})]. \qquad (16)$$

The flux of a given species through the boundary layer is equal to the product of its mass-transfer coefficient and the difference in its partial pressure on the two sides of the boundary layer [13]. Since the gas in the experimental apparatus (see Chapter III) is being continuously circulated through the oxidation region while the oxide species are being continuously removed it is logical to assume that the partial pressure of each of the oxide species in the free stream approaching the wire is negligible with respect to its partial pressure at the inner surface of the boundary layer. Thus, the diffusion flux of the species is equal to the product of its mass-transfer coefficient and its partial pressure at the inner surface of the boundary layer. Therefore, the surface recession rate of the metal due to the diffusion of $IrO_2(g)$ can be expressed by

$$\dot{X}_{D2} = A\, k_{G2}P_{2S} \qquad (17)$$

where k_{G2} is the mass-transfer coefficient of $IrO_2(g)$.

It will be assumed that there are negligible rates of net reactions between the oxide species and other species in the boundary

layer. This allows equating $\dot{X}_{D2}$ to $\dot{X}_{S2}$. Then Eqs. (16) and (17) can be solved for P_{2S} and $\dot{X}_{S2}$. The resultant expression for the surface recession rate is

$$\dot{X}_{D2} = \dot{X}_{S2} = \dot{X}_2 = \frac{Ak_{G2} K_2 P_{O_2} (2\pi M_2 RT_k)^{-1/2}}{k_{G2} + (2\pi M_2 RT_k)^{-1/2}} . \qquad (18)$$

where $\dot{X}_2$ is just a simpler notation for the surface recession rate component dependent on the evaporation and diffusion of $IrO_2(g)$.

Analogous mathematical treatment of the formation and diffusion of the $IrO_3(g)$ and Ir(g) species results in similar expressions for $\dot{X}_3$ and $\dot{X}_M$ where the subscript 3 refers to the quantity pertaining to $IrO_3(g)$ and the subscript M refers to the quantity pertaining to Ir(g). If it is now assumed that the total surface recession rate of the metal is the sum of the recession rates for each independent oxide species, then

$$\dot{X} = \dot{X}_2 + \dot{X}_3 + \dot{X}_M \qquad (19)$$

or

$$\dot{X} = A\left[\frac{k_{G2}\,K_2\,P_{O_2}(2\pi M_2 RT_k)^{-1/2}}{k_{G2} + (2\pi M_2 RT_k)^{-1/2}} + \frac{k_{G3}\,K_3\,P_{O_2}^{3/2}(2\pi M_3 RT_k)^{-1/2}}{k_{G2} + (2\pi M_3 RT_k)^{-1/2}} + \frac{k_{GM}\,P_M\,(2\pi M_M RT_k)^{-1/2}}{k_{GM} + (2\pi M_M RT_k)^{-1/2}}\right] \quad (20)$$

where k_{G3}, K_3, and M_3 are respectively, the mass transfer coefficient, equilibrium constant, and molecular weight of $IrO_3(g)$ and k_{GM}, P_M, and M_M are respectively, the mass transfer coefficient, partial pressure, and atomic weight of Ir(g).

Equation (20), which predicts surface recession rates, was considered to be a complete description of the oxidation/evaporation of iridium wires. The validity of this theoretical development was tested by correlating the surface recession rates which were calculated by Eq. (20) with experimentally determined surface recession rates.

CHAPTER III

EXPERIMENTAL PROCEDURES FOR NATURAL-CONVECTION REGIME

Experimental Materials

The iridium wire used in this study was commercially pure and was purchased in four separate lots which have been labeled Lot 1, Lot 2, Lot 3, and Lot 4. A previous study by Kraus [11] utilized Lots 1 and 2 and the study by Wahl [9] incorporated wire from Lots 1, 2, and 3. The major impurities in the wire of the first three lots have been tabulated [9] and Lot 1 was estimated to be 99.3 percent pure while Lots 2 and 3 were estimated to be 99.9 percent pure. Lot 4 is of similar composition and is estimated to be 99.9 percent pure also. It has been shown [8, 9, 11] that no perceptible differences exist between the oxidation rates of Lots 1, 2, and 3. Thus, Lot 4 is expected to react similarly.

The oxygen used was USP grade and was typically 99.7 percent pure. Nitrogen and argon were the primary impurities and were both expected to be inert to iridium. Both the oxygen and the air were dried before they entered the oxidation chamber so water vapor was not expected to be a contributing part of the oxidation atmosphere.

Apparatus and Procedure

The equipment that was used to experimentally determine oxidation rates of iridium was the same apparatus described in detail by Wahl [9].

A schematic representation of the system is shown in Fig. 1. It basically consists of a water cooled oxidation cell in which the iridium wire is suspended horizontally between two water cooled electrodes. The cell was provided with two sight ports containing rotatable pyrex windows. Through one port an optical pyrometer was sighted on the wire and a timer-actuated, motor-driven camera fitted with a telemicroscope was focused on the same point of the wire through the other window. The optical pyrometer was calibrated [9] to read the true wire temperature through the optical quality pyrex windows. Rotation of the windows (to a clean section) just prior to taking a temperature measurement insured reading the true temperature of the wire since the part of the window which was exposed to the oxidation atmosphere would collect iridium oxide condensate.

The pressure in the cell was measured by a capacitance manometer for pressures greater than 1.32×10^{-4} atm (0.10 torr) and by a high pressure ion guage for pressures less than 1.32×10^{-4} atm (0.10 torr). Either one of these systems could be used to signal an automatic pressure controller which controlled a servo-valve regulating the flow of gas into the system. With the system being vacuum pumped continuously, a constant flow of gas insured that the atmosphere in the cell did not contain a high percentage of oxide species. A more detailed description of this apparatus is given by Wahl [9].

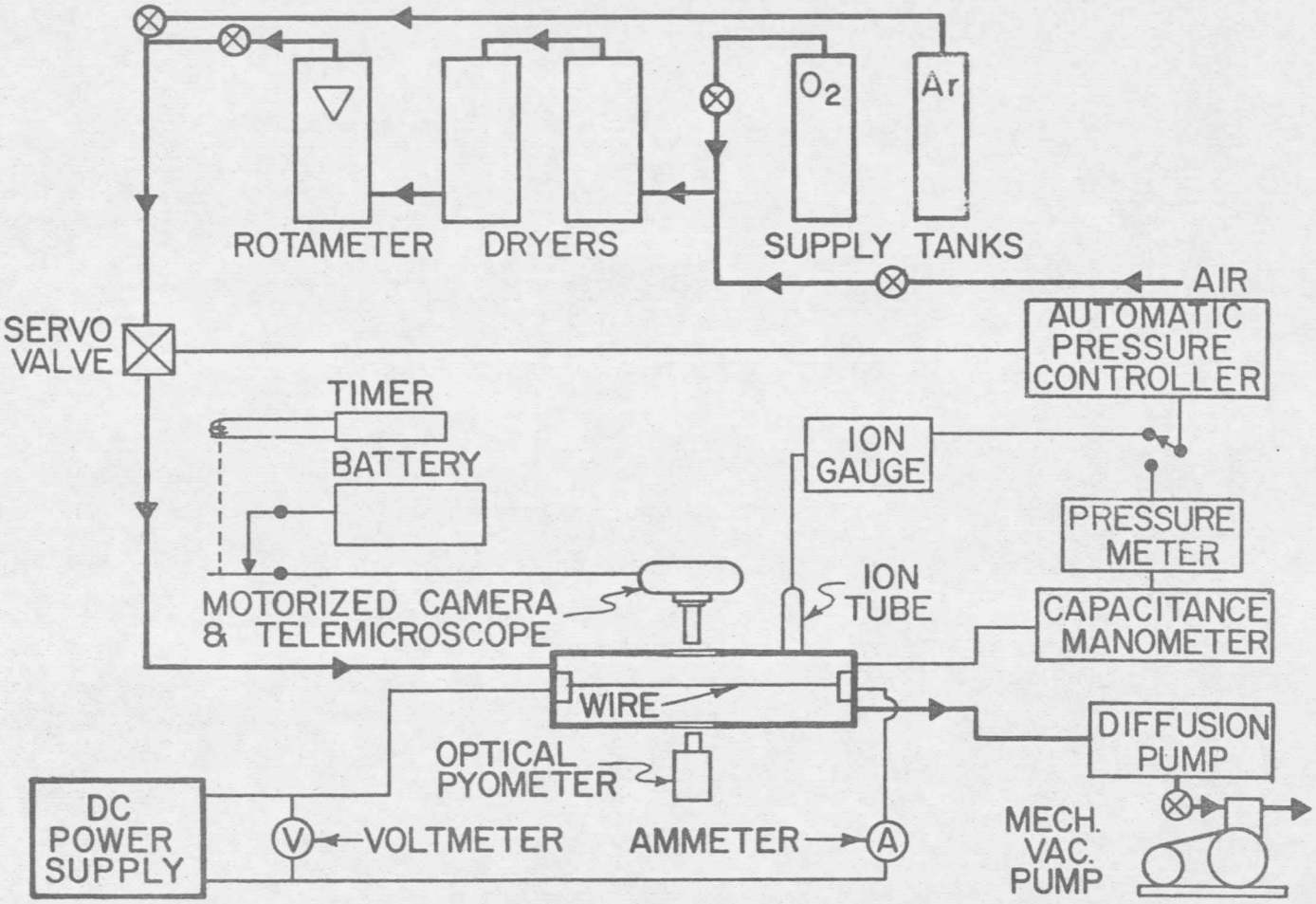

Figure 1: Schematic Representation of Natural-Convection Oxidation Apparatus

Prior to mounting a section of wire in the oxidation cell the wire was thoroughly cleaned in acetone to remove any surface deposits. After the wire was mounted between the electrodes it was annealed for 30 minutes at 2260°C (2533°K) in an argon atmosphere. The annealing eliminated any further recrystallization or grain growth occurring after the oxidation run started. After the argon was removed and the pressure of the flowing gas was stabilized at the preselected value the wire was brought to the desired temperature by self resistance heating caused by passing an electric current through it. As the temperature of the wire was monitored through the optical pyrometer a series of 10 film images of the hot wire was obtained. The time interval between the images was selected so that approximately 0.025 mm (1 mil) was removed from the diameter of the wire during each run.

On each film an exposure was made of a drill rod of known diameter at the same focal length as the oxidizing wire. After the film was developed and dried this image provided a reference of known diameter on the film. The film images of the wire were measured by a modified cathetometer in which a foil with a 0.05 mm (2 mil) slit was incorporated in the telemicroscope. By means of a high intensity light behind the film and a light meter on the eyepiece of the cathetometer the diameter of the film images could be determined and converted to an actual wire diameter by a conversion factor obtained from the image of the known diameter rod. The repeatability of a

single measurement was typically $\pm$ 0.05 to 0.1 percent. However, it was found that a minor correction must be made for the variation of the width of the fringe zone located at the edge of the film image (as viewed at 40x magnification through the cathetometer) with change in the wire temperature. This correction factor was determined by heating a wire in argon to the same temperatures used in the oxidation runs and taking photographs in the same manner as was done in the oxidation experiments. After this wire was cooled it was taken from the cell and measured directly by the cathetometer. Correction of this diameter for thermal expansion at the various temperature levels then allowed the comparison of the wire diameters as measured from the film by the previously mentioned procedure to the actual wire diameters.

The improved method of temperature measurement [9] was applied to a previous study of the thermal expansion of iridium [14] and new coefficients in the equation for the expansion of iridium were derived. "Percent expansion" is defined as 100 times the increase in length at T_c (°C) divided by the length at 0°C. The new equation is

$$\text{Percent Expansion} = 6.646 \times 10^{-4}\, T_c - 2.69 \times 10^{-8}\, T_c^2 + 1.533 \times 10^{-10}\, T_c^3 - 3.506 \times 10^{-14}\, T_c^4. \quad (21)$$

For the temperature range of 440 to 2220°C (713 to 2493°K) the maximum disparity between Eq. (21) and the experimental data was 2.63 percent of the experimentally determined percent expansion.

CHAPTER IV

RESULTS AND DISCUSSION OF NATURAL-CONVECTION OXIDATION

Experimental Data

After the actual diameter of the wire had been determined from the film measurements the diameter of the wire at each exposure was plotted versus the time elapsed from the first exposure of the run. Fig. 2 shows a typical plot which resulted from this procedure. As was noted earlier, the oxidation of iridium at these elevated temperatures is linear with respect to time since the oxides are all volatile and no protective coating is formed on the surface. The slope of this line is the negative of the rate of decrease of the diameter of the wire. Therefore the surface recession rate of the metal can be found by multiplying the slope of the line by minus one half. Since the calculations for finding the theoretical rate involve the wire diameter, an average diameter for each run was taken as the average of the ten diameters read from each film. Tables (6) and (7) in Appendix A give the experimental conditions and the experimentally determined oxidation rates for the oxidation of iridium in pure oxygen and air. As is noted, most of these data were gathered by Kraus [11] and Wahl [9] but their diameter measurements were modified because of the film image fringe effect discussed earlier. The calculated values on these tables were calculated by Eq. (20).

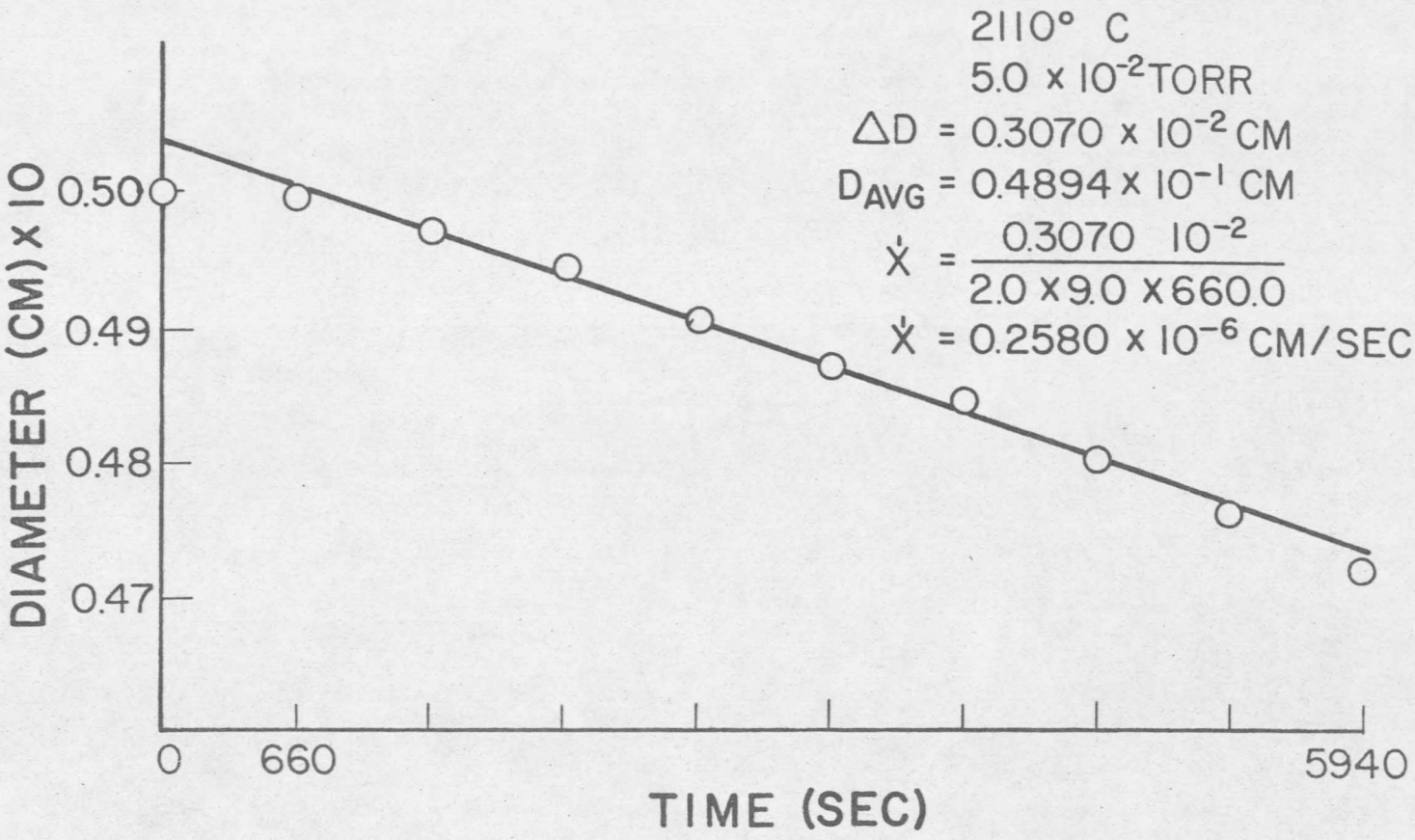

Figure 2: Example of a Rate Plot from a Typical Oxidation Experiment

Figures 3 and 4 show the correlation of the theoretical results with the experimental results. Equation (20) is represented for each temperature level by the solid line and the experimental points are plotted by their respective symbol for each temperature level and lot number. In Fig. 3 some of the data at the intermediate temperatures were omitted so as to avoid confusion in examining the plot. In calculating values to plot Eq. (20) an average diameter of all of the experimental runs was used. Tables 1 and 2 also show the effectiveness of the theoretical correlation by giving the average absolute values of the deviations of Eq. (20) from the experimental data for each temperature level.

Calculation of Theoretical Rates

The mass transfer coefficient for each diffusing species was calculated by means of the following expression from the Chilton-Colburn equations [13]:

$$k_{Gi} = \frac{hP}{RT_f C_p \rho P_{BM}} \left(\frac{C_p \rho D_{vi}}{k} \right)^{2/3} \qquad (22)$$

where h is the convective heat transfer coefficient, P is the total pressure, C_p is the specific heat of the matrix gas (oxygen or air) at constant pressure, ρ is the density of the matrix gas, D_{vi} is the

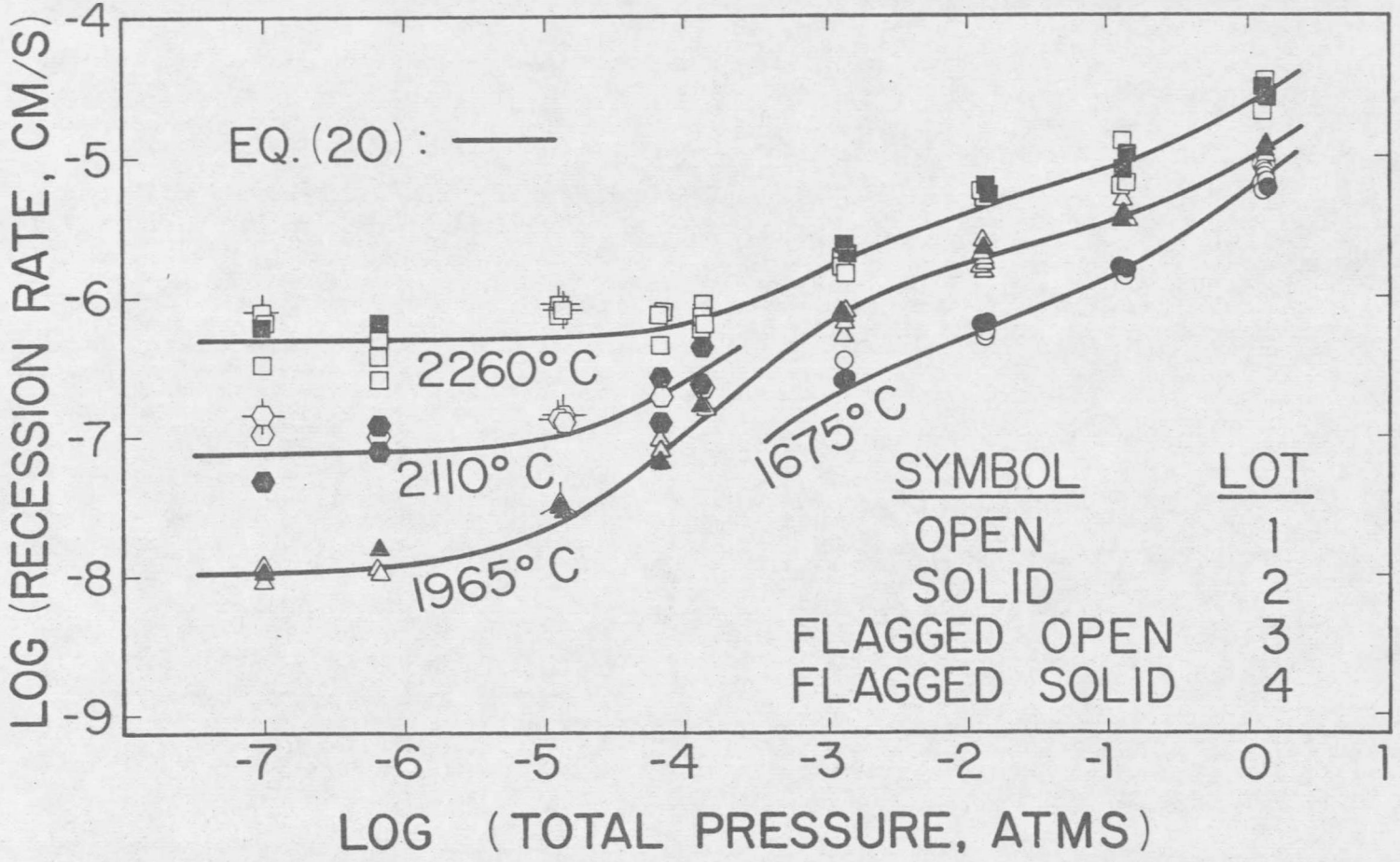

Figure 3: Experimental Results and Theoretical Correlation for Naturally Convected Oxidation in Pure Oxygen

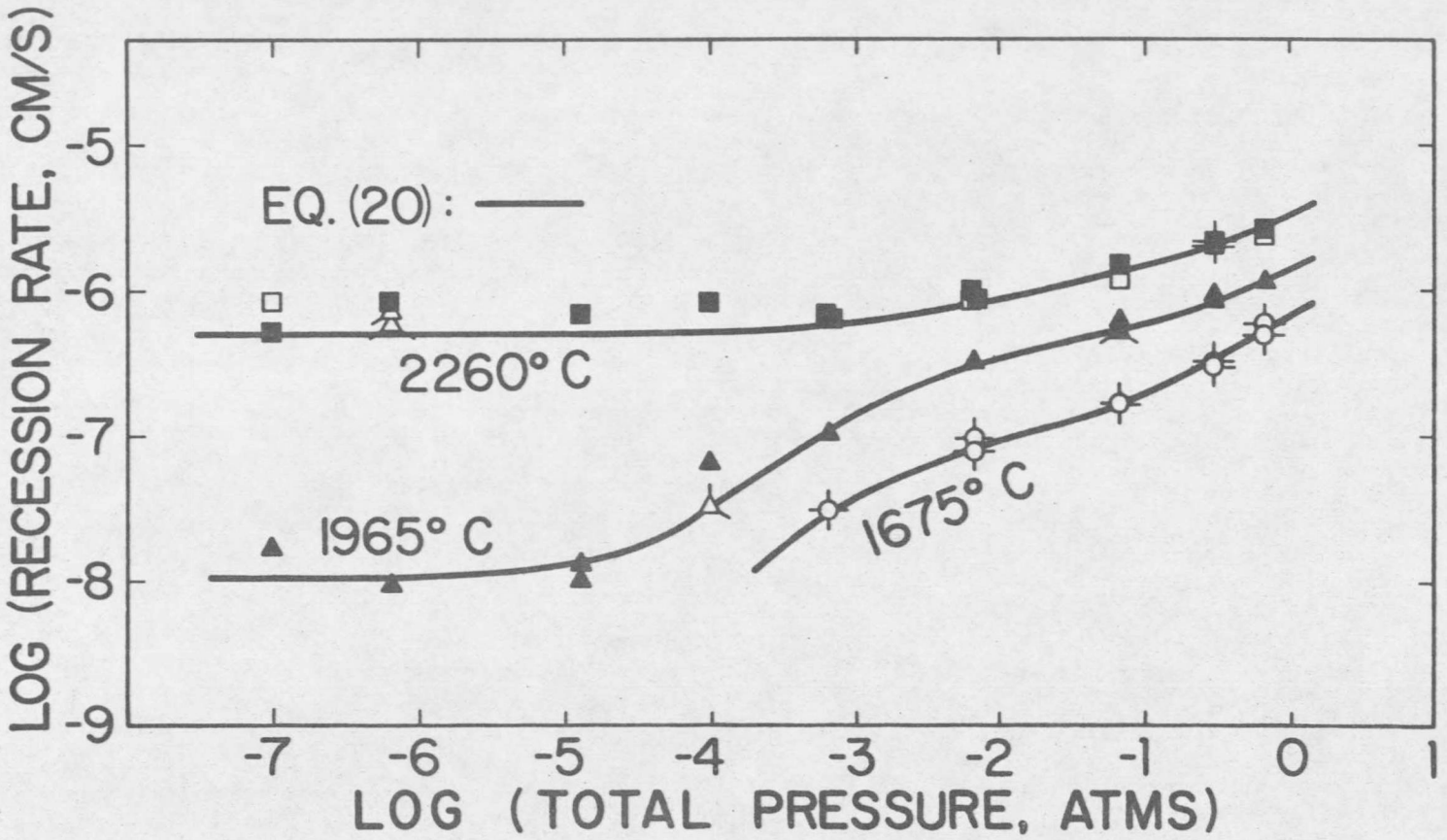

Figure 4: Experimental Results and Theoretical Correlation for Naturally Convected Oxidation in Air

TABLE 1

Average Deviation of Theoretical Equation from Experimental Data for Naturally Convected Oxidation in Pure Oxygen.

Wire Temp. (°C)	Average Deviation (%)
1675	9.07
1820	6.78
1965	11.49
2110	21.14
2260	22.35
Overall Average:	15.88

TABLE 2

Average Deviation of Theoretical Equation from Experimental Data for Naturally Convected Oxidation in Air.

Wire Temp. (°C)	Average Deviation (%)
1675	8.65
1820	3.32
1965	13.61
2110	7.40
2260	18.11
Overall Average:	13.11

gaseous diffusivity for the ith species, T_f is the absolute film temperature, P_{BM} is the logarithmic mean pressure of the nondiffusing matrix gas (thus $P \simeq P_{BM}$, since the partial pressure of the oxide species is small), and k is the thermal conductivity of the matrix gas. All of the above properties of the matrix gas were evaluated at the film temperature which is equal to the average of the wire temperature and the ambient free-stream temperature. The Chilton-Colburn equations used in obtaining Eq. (22) are valid for Prandtl numbers ($C_p\mu/k$, where μ is the viscosity of the gas) in the range of 0.6 to 100 and Schmidt numbers ($\mu/\rho D_{vi}$) in the range of 0.6 to 2500 [15]. The ranges of the Prandtl and Schmidt numbers in this study were 0.720 to 0.732 and 1.39 to 2.01, respectively.

Values for the convective heat transfer coefficient, h, were calculated from the Madden-Piret [16] general equation for heat transfer from horizontal wires that is of the form

$$Nu = \frac{hD}{k} = \frac{2}{C_1(8k\gamma\lambda)/(\mu C_p[\gamma+1]D) - C_2 \ell n(1+2\lambda/D) + C_2\phi} \qquad (23)$$

where

$$C_1 = \frac{k_{w,a}}{\alpha k_{w,\lambda}}, \qquad C_2 = \frac{k_{w,a}}{k_{\lambda,a}}, \qquad (24), \quad (25)$$

γ is the specific heat ratio for the matrix gas, λ is the mean free path of the matrix gas, and α is the thermal accomodation coefficient

for energy exchange between the iridium surface and the matrix gas molecules. In Eqs. (24) and (25) $k_{w,a}$ is the thermal conductivity of the matrix gas evaluated at the mean of the temperatures of the wire (subscript w) and the ambient (subscript a). Similarly, the subscript λ refers to a location one mean free path away from the surface of the wire. The first two terms in the denominator of Eq. (23) are important for low pressure conditions while the heat transfer in the continuum regime is represented by ϕ. For horizontal wires Madden and Piret [16] found this to be

$$\phi = \ell n(6.82\ Ra^{-1/3}) \tag{26}$$

where Ra is the Rayleigh number, which is

$$Ra = g\rho^2 D^3 \beta C_p [\Delta T]/\mu k \tag{27}$$

where g is the gravitational acceleration, β is the ocefficient of expansion for the matrix gas (which is the reciprocal of the absolute temperature for an ideal gas), and ΔT is the temperature difference between the wire and the ambient gas.

In the experimental work which Madden and Piret performed the values of ΔT were limited to 65°C (65°K) which allowed them to conveniently set the thermal conductivity ratios in Eqs. (24) and (25) to unity. Since the temperature differences in this study were much larger, these ratios cannot be assumed unity. The constants C_1 and C_2

are not readily calculable because the temperature at a distance one mean free path from the wire is unknown. The larger ΔT's also prohibit the use of Eq. (26) so it was decided to attempt to experimentally determine the values of ϕ, C_1, and C_2.

It was assumed that the mean free path of the gas becomes negligibly small at pressures greater than about 0.2 atm (150 torr). This assumption agrees with Aihara and Koyama's [17] observation of continuum behavior at low Reynolds numbers (3×10^{-3} to 2×10^{-1}) and pressures in the range of 0.26 to 1.0 atm (200 to 760 torr). If this assumption is applied to Eq. (23) the first two terms in the denominator become negligible with respect to the third. Also, for a small mean free path, $k_{\lambda,a} \simeq k_{w,a}$ and C_2 becomes unity. Therefore, for the following heat transfer study, Eq. (23) becomes

$$Nu = \frac{h\,D}{k} = \frac{2}{\phi} \,. \tag{28}$$

A new equation for ϕ was obtained by correlating a series of measurements of the rates of heat transfer from an iridium wire in the oxidation cell in an argon atmosphere. The pressures of this study ranged from 0.27 to 1.25 atm (205 to 950 torr). Heat transfer rates per unit length of wire in the constant temperature zone were calculated from values of the diameter (measured photographically as in the oxidation experiments), the current (measured to $\pm$ 0.01 amp

using a precision shunt and digital millivoltmeter), and the high temperature resistivity of iridium [18]. Heat transfer rates were also measured at 10^{-8} atm (8×10^{-6} torr) and these rates were subtracted from the rates measured at higher pressures in order to correct for the radiant component of heat transfer. The final results of this heat transfer study were empirically correlated to yield

$$\phi = \ell n[8.87 Ra^{-0.354}(T_k/T_a)^{-0.464}] \qquad (29)$$

where T_k is the absolute temperature of the wire and T_a is the absolute ambient temperature.

Values for the gaseous diffusivity, D_{vi}, in Eq. (22) were calculated by means of the Wilke-Lee modification of the Hirschfelder-Bird-Spotz equation [19]. The value of 33 cm^3/g-atom obtained by Wimber and Kraus [8] for the atomic volume of iridium was used in calculating the collision diameters. The interaction energies were calculated by empirical equations given as 1.92 times the absolute melting temperature of the respective oxide species [19].

P_M, the partial pressure of the iridium metal, was calculated from the empirical vapor pressure equation of Honig and Kramer [20]. This equation is

$$\log [760\ P_M] = -8464.67/T_k + 65.5812 \log(T_k) - 0.0100272\ T_k + 5.44981 \times 10^{-7}\ T_k^2 \qquad (30)$$

where P_M is the vapor pressure of the metal in atmospheres. The properties of the gases were taken from NBS tables [21] and were fitted to empirical equations over the temperature range of this study by a least squares curve-fitting technique. The resulting equations are summarized in Tables 3 and 4.

Now all but six of the parameters needed to calculate oxidation rates from Eq. (20) are known or can be calculated. The unknown entities are the melting points of IrO_2 and IrO_3, the two coefficients C_1 and C_2 in Eq. (23), and the two equilibrium constants K_2 and K_3. These six quantities were treated as unknowns in Eq. (20) and were subsequently found as Eq. (20) was correlated with the experimental data.

As was discussed previously, the coefficients C_1 and C_2 become negligible at pressures greater than about 0.2 atm (150 torr). Therefore if Eq. (20) is correlated with the data which was obtained at pressures above this value there will be only four unknowns to consider. Two of these unknowns are the melting temperatures of the oxides. No information could be found about the melting point of IrO_3, but it is known that the melting point of IrO_2 must be in excess of 1383°K [22, 23]. For lack of better information a common value was

TABLE 3

Properties of Oxygen
$1000°K \leq T_f \leq 1400°K$

Property	Relation	Units
Density	$\rho = 0.3899\ P/T_f$	gm/cm^3
Specific Heat	$C_p = 0.116\ T_f^{0.117}$	cal/gm/°K
Viscosity	$\mu = 5.374 \times 10^{-6} T_f^{0.650}$	gm/sec/cm
Thermal Conductivity	$k = 8.12 \times 10^{-7} T_f^{0.7738}$	cal/cm/sec/°K
Specific Heat Ratio	$\gamma = 1.682\ T_f^{-0.0359}$	--
Mean Free Path	$\lambda = 1.074 \times 10^{-8} T_f^{1.15}/P$	cm

NOTE: P is the total pressure in atmospheres

T_f is the film temperature in °K

TABLE 4

Properties of Air
$1000°K \leq T_f \leq 1400°K$

Property	Relation	Units
Density	$\rho = 0.3530\ P/T_f$	gm/cm^3
Specific Heat	$C_p = 0.0773\ T_f^{0.1825}$	cal/gm/°K
Viscosity	$\mu = 7.313 \times 10^{-6} T_f^{0.5849}$	gm/sec/cm
Thermal Conductivity	$k = 1.239 \times 10^{-6} T_f^{0.7023}$	cal/cm/sec/°K
Specific Heat Ratio	$\gamma = 2.001\ T_f^{-0.0585}$	--
Mean Free Path	$\lambda = 1.5347 \times 10^{-8} T_f^{1.0849}/P$	cm

NOTE: P is the total pressure in atmospheres

T_f is the film temperature in °K

assigned to the melting points of the two oxides and was incremented in 100°K steps over the range of 1400 to 2400°K in view of the general range of melting/decomposition temperatures of heavy metal oxides having appreciable volatility [24]. For each assumed value of the oxide melting temperature the experimental oxidation rates were equated to the right hand side of Eq. (20) and values of K_2 and K_3 were simultaneously calculated for each temperature level to yield the closest correlation of Eq. (20) to the experimental data (by least squares curve-fitting, using double precision programming with a Xerox Sigma 7 digital computer). At each experimental temperature level for each value of the oxide melting point the disparity between the experimental oxidation rate and the rate calculated by Eq. (20) using the newly found values of K_2 and K_3 was calculated. It was observed that this correlation disparity was very insensitive to the value of the oxide melting point; in fact, the average of the disparities for the five experimental temperature levels was constant to three significant figures over the entire incrementation of the oxide melting temperature (1400 to 2400°K). In view of the insensitivity of the equilibrium constants to variation of the oxide melting point the melting temperature of the oxides was assigned an average value of 1900°K and was assumed constant for all subsequent calculations.

From the values of K_2 and K_3 obtained at each of the experimental oxidation temperatures the standard-state free-energies of formation

were calculated and these values were least squares curve-fitted as a function of the absolute wire temperature. The equations for the two oxides are

$$\Delta F_f^\circ[IrO_2(g)] = 11295 - 20.507\ T_k + 0.013971\ T_k^2 - 4.2208 \times 10^{-6}\ T_k^3 + 4.7700 \times 10^{-10}\ T_k^4 \quad (31)$$

and

$$\Delta F_f^\circ[IrO_3(g)] = -19266 + 35.501\ T_k - 0.024457\ T_k^2 + 7.4722 \times 10^{-6}\ T_k^3 - 8.5398 \times 10^{-10}\ T_k^4 \quad (32)$$

where the units of the ΔF's are kcal/mole. Figure 5 contains a plot of Eqs. (31) and (32) superimposed on the experimentally determined values of K_2 and K_3. Also shown in Fig. 5 are the results of mass spectrometric studies made by Olivei [7] and Norman, et al [6]. Olivei's results were extrapolated to 2500°K from data taken in the range of 1000 to 1800°K and in view of the uncertainties reported in each case the results of the present study appear to be in fairly good agreement.

Now that an approximate value for the melting temperatures of the oxides has been assumed and values for the equilibrium constants were calculated by the use of Eqs. (31) and (32) the theoretical correlation was extended to the entire pressure range and values for the coefficients C_1 and C_2 were found in a similar manner. Again, Eq.

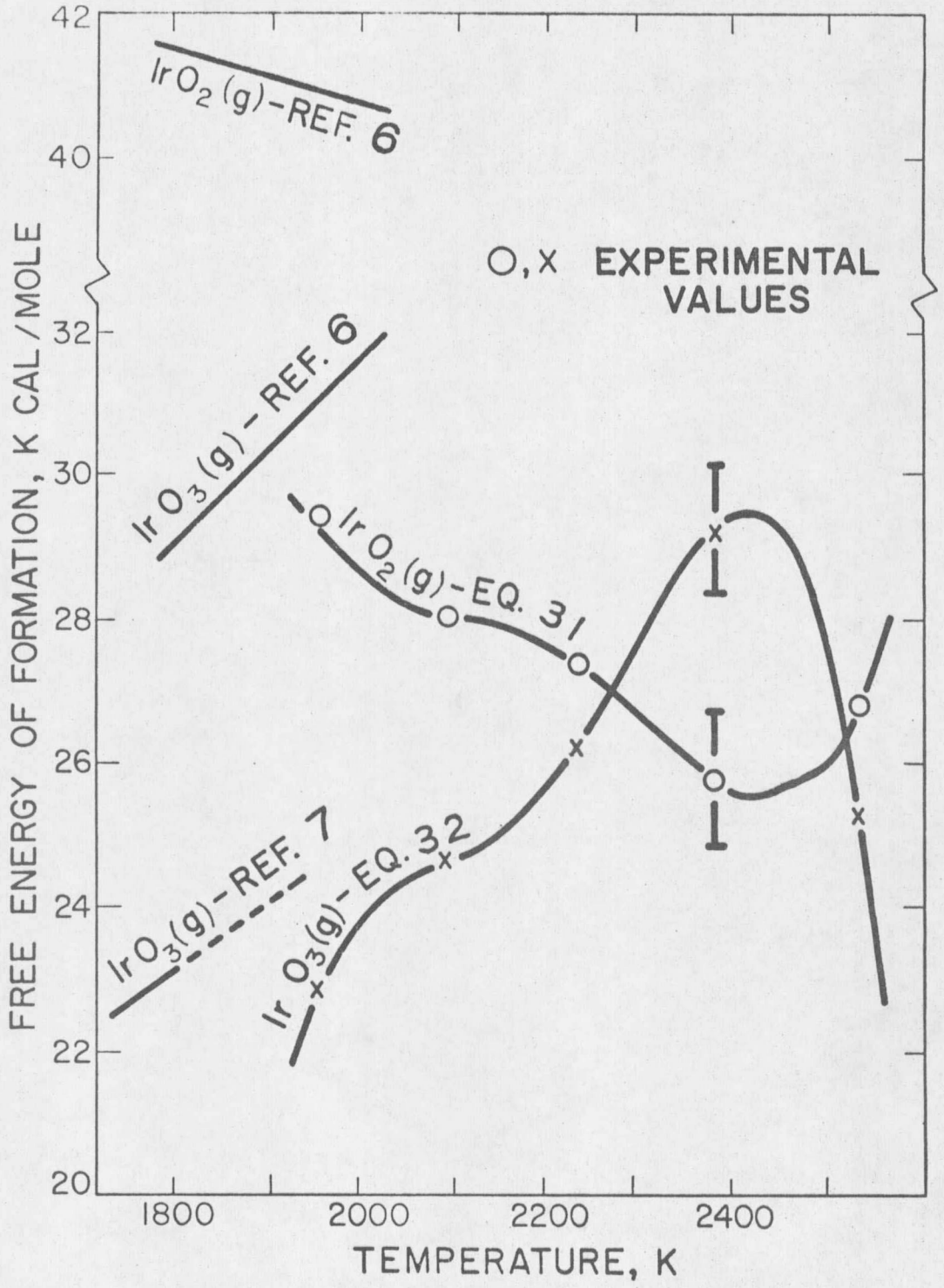

Figure 5: Resultant Free Energies of Formation

(20) was correlated with the experimental data and optimized for values of C_1 and C_2. The ranges of these values for C_1 and C_2 over the range of experimental temperature levels were 0.29 to 0.84 and 1.02 to 1.05, respectively and were seen to be in agreement with the anticipated limits of these two quantities [16]. Least squares curve-fitting of these two parameters so as to minimize the correlation disparity resulted in the following equations:

$$C_1 = 180.03 - 0.23691\ T_k + 1.0005 \times 10^{-4}\ T_k^2 - 1.2217 \times 10^{-8}\ T_k^3 - 5.4490 \times 10^{-13}\ T_k^4 \qquad (33)$$

$$C_2 = 1.538 - 5.397 \times 10^{-4} T_k + 1.366 \times 10^{-7} T_k^2. \qquad (34)$$

With all these quantities known or calculable, oxidation rates were calculated from Eq. (20). Tables 1 and 2 showed the average deviations of the theoretically determined rates from the experimentally determined rates. A logical comparison with these percentages of deviation would be the percentage of experimental scatter. In this case the experimental scatter is difficult to evaluate because the rate of oxidation is dependent on the wire diameter which varied with each experiment. Kraus [11] derived a method of determining "approximate experimental scatter" for his data of oxidation in pure oxygen. For the data of oxidation in oxygen this

method gives the following values for the approximate experimental scatter:

at 1675°C - - - 5.3%,

at 1820°C - - - 4.4%,

at 1965°C - - - 7.1%,

at 2110°C - - -15.4%,

at 2260°C - - -15.5%,

Overall Average: 8.8%.

Comparison of these values to the deviations of Table 1 reveals that the correlation is quite effective. The "overall average" which is tabulated here and in Tables (1) and (2) is not the average of the five numbers presented but is the average of all the runs made since the numbers of runs made at each temperature level are not equal. The data for oxidation in air were not numerous enough to calculate an experimental scatter but it is expected that the correlation is of equal quality for oxidation in air.

CHAPTER V

EXPERIMENTAL PROCEDURES FOR FORCED CONVECTION REGIME

Experimental Materials

All of the materials used in this portion of the study were the same as used in the natural-convection regime. For a discussion on this see Chapter III.

Apparatus and Procedure

The study in force convected air and oxygen was separated into two parts; one for low Reynolds numbers (Re < 15), and one for high Reynolds numbers (Re > 20). The apparatus for experimentally determining oxidation rates at the low Reynolds numbers was described in detail by Tempero [25]. This equipment consisted basically of a nozzle injector mounted on the top of the oxidizing cell which was used in the natural convection work. The injector was constructed of a 7 cm ID circular cylinder in which there was a baffle and a series of stainless steel screens which were provided to eliminate turbulence caused by the gas stream initially entering the apparatus. The series of screens was composed of one 20-mesh screen, two 40-mesh screens, and one final 100-mesh screen. After the gas had passed through these screens it entered a convergent section which terminated in a nozzle having an inside diameter of 2.22 cm. This nozzle was positioned approximately one-eighth inch above the center of the oxidizing wire.

Hot-wire-anemometry work was conducted [1] with the injector in place to determine velocity profiles under various flow and pressure conditions. The turbulence level was found to be less than or equal to one percent over the range of flow conditions studied and the diameter of the constant velocity region was never less than 0.65 cm. A ratio of the center line velocity to the area averaged velocity was also measured so the center line velocity could later be calculated from the volumetric flow of the gas. The volumetric flow was measured during each experimental run with one of three different rotameters [25].

The temperatures at which the wires were oxidized were the same as utilized in the natural convection study and the pressures were in the range of 0.0046 to 1.32 atm (3.5 to 1000 torr). The Reynolds numbers ranged from 0.064 to 12.03. In this low Reynolds number study the only gas used was pure oxygen.

The diameters of the oxidizing wires were measured photographically as in the previous discussion but additional photographs were taken of the wire before and after each run to see if the wire oxidized asymmetrically. These photographs were taken at 45° increments of rotation at the point on the wire where the center of the oxygen stream was positioned.

The apparatus for oxidation experiments at higher Reynolds numbers involved the same nozzle as previously discussed but it was modified

so that it terminated in a nozzle having an inside diameter of 0.635 cm. However, this nozzle was not mounted on the oxidation cell which was used before but it was simply mounted in the atmosphere. Similar hot-wire-anemometry work was conducted for this nozzle and it was determined that the turbulence level was always less than or equal to 1.2 percent. The velocity profile showed that the velocity was constant to within one percent over the central 0.45 cm portion of the diameter. Again the ratio of the center line velocity to the area averaged velocity allowed calculation of the centerline velocity from the volumetric flow rate. In this apparatus the volumetric flow rates were measured by a Meriam laminar flow element and were corrected for temperature and pressure of the flowing stream.

The mounting bracket for the nozzle included two water cooled electrodes between which a 1.5 cm section of wire could be mounted. The wire was mounted vertically and clamped at one end while suspended in a pool of mercury at the other end. The mercury pool electrode allowed thermal expansion of the wire without deflection. The power source used was the same DC supply which was used in the natural-convection studies. The temperature was also monitored by the same optical pyrometer as in the natural-convection study. Diameters of the oxidizing wires were measured in the same manner with the same camera system as used in the natural-convection study and the low Reynolds number forced convection study. Again, photographs were

taken at 45° increments of rotation before and after each oxidation run.

The specimens were oxidized at high Reynolds numbers in both oxygen and air. Since the experiments were not performed in a closed container the pressure was the current atmospheric pressure which ranged from 0.82 to 0.84 atm. The Reynolds numbers in this portion of the study ranged from 22.98 to 600.6.

CHAPTER VI

RESULTS AND DISCUSSION OF FORCED CONVECTION OXIDATION

Experimental Data

The results of the low Reynolds number oxidation study are tabulated in Table 8 in Appendix B. These are the data gathered by Tempero [25] which were corrected for temperature measurement and diameter measurement. The experimental conditions and experimentally determined oxidation rates are tabulated with the oxidation rates calculated by Eq. (20). The average deviation of the calculated values from the experimental values were calculated and are presented in Table 5. No average deviation values are given for the intermediate temperatures of 1820 and 2110°C because only one run was made at each level. The overall average of the deviation is the average of all the data points and not the average of the three numbers presented.

The results of the high Reynolds number oxidation study are presented in Table 9 in Appendix B. When the first five experimental runs were performed for this part of the study the rotational photographs before and after oxidation were not included. Later it was discovered that the wire did oxidize asymmetrically and this procedure was followed for subsequent runs. Therefore the diameter correction factor and the rate correction factor for the first five runs in Table 9 were not determined experimentally but were calculated

TABLE 5

Average Deviation of Theoretical Equation from Experimental Data for Force-Convected Oxidation at Low Reynolds Numbers in Pure Oxygen

Wire Temp. (°C)	Average Deviation (%)
1675	5.48
1965	6.95
2260	8.58
Overall Average:	7.76

by Eqs. (42) and (43). The last two runs of Table 9 were performed in pure oxygen whereas all the others were in air. Average deviations for each temperature level were not calculated because the data were too few, but the overall average deviation of all the runs is 21.44 percent.

Calculation of Theoretical Rates

In calculating the theoretical rates for forced convection oxidation by Eq. (20) all the parameters were considered to be the same as for natural convection except the mass transfer coefficient which is dependent on the convective heat transfer coefficient. In reviewing the literature it was noted that for large temperature differences the Nusselt number was not a function of Reynolds number alone but was usually expressed as a function of Reynolds number and a temperature ratio. The temperature ratio was either a ratio of absolute wire temperature to absolute ambient temperature [26] or a ratio of absolute film temperature to absolute ambient temperature [27]. In this study the equation which was used to calculate the Nusselt numbers for all data in the forced convection regime was developed by Fand and Keswani [27] and is expressed by

$$Nu = (T_f/T_a)^{0.17} (0.184 + 0.324\ Re^{1/2} + 0.291\ Re^{x}) \quad (35)$$

where $x = 0.247 + 0.0407\ Re^{0.168}$ and all the gas properties were evaluated at the absolute film temperature (T_f).

At the low Reynolds number oxidation it was determined by Tempero [25] that the oxidized wires were approximately circular and the extent of asymmetry was less than five percent in all cases. Therefore this effect was neglected and, in calculating the theoretical rates that appear in Table 8, the convective heat transfer coefficient was evaluated directly from Eq. (35) and all other parameters needed for Eq. (20) were found as described in Chapter IV.

At the high Reynolds number oxidation it was found that the wire cross sections were not circular after oxidation. The apparatus was arranged such that during each experimental run the wire diameters (and subsequently the oxidation rates) were measured in the direction of the gas flow. Therefore, in order to calculate theoretical rates, "circumferentially averaged" wire diameters, Reynolds numbers, and Nusselt numbers were needed and then these calculated rates were compared to the circumferentially averaged experimental rates.

The average wire diameter for each run was taken to be the average of the circumferentially averaged diameter before the oxidation and the circumferentially averaged diameter after the oxidation. This is expressed

$$D_{AV} = (1/8)[(D_0+D_{45}+D_{90}+D_{135})_b + (D_0+D_{45}+D_{90}+D_{135})_a] \qquad (36)$$

where the subscripts b and a refer to before and after the run, respectively, and the subscripts 0, 45, 90, and 135 refer the the degree increments of rotation around the wire where 0° corresponds to the axis which is parallel to the flow of gas. It was desirable for computer programing to be able to calculate the overall average diameter from the average diameter of the measurements which were used in the rate plots (as in Fig. 2). The diameters used in the rate plots were all measured in the flow direction (0°) and the resultant expression for the average diameter is

$$D_{AV} = C_D D_R \tag{37}$$

where D_R is the average diameter from the rate plots, and the correction factor for diameter, C_D, can be expressed as

$$C_D = \frac{(D_0+D_{45}+D_{90}+D_{135})_b + (D_0+D_{45}+D_{90}+D_{135})_a}{4(D_{0b}+D_{0a})} . \tag{38}$$

Therefore C_D was determined experimentally from the rotational photographs taken before and after each oxidation run. These values are tabulated in Table 9. With the circumferentially averaged diameters known, the resultant Reynolds numbers were calculated and the subsequent Nusselt numbers yielded the average convective heat transfer coefficients. Calculation of the theoretical rates was then accomplished by using these values in Eq. (20).

To compare these rates calculated by Eq. (20) to the experimental rates, circumferentially averaged experimental rates must be found. The surface recession rate of the wire is directly proportional to the change in diameter. The overall average change in diameter can be expressed as

$$\Delta D_{AV} = (1/4)[(D_0+D_{45}+D_{90}+D_{135})_b - (D_0+D_{45}+D_{90}+D_{135})_a]. \quad (39)$$

Since the measured rate is in the flow direction, the circumferentially averaged rate can be expressed as

$$\dot{X}_{AV} = C_R \dot{X}_R \quad (40)$$

where $\dot{X}_R$ is the rate determined from the rate plot and the rate correction factor is

$$C_R = \frac{(D_0+D_{45}+D_{90}+D_{135})_b - (D_0+D_{45}+D_{90}+D_{135})_a}{4(D_{0b} - D_{0a})}. \quad (41)$$

The data presented in Table 9 include these correction factors and the corrected diameters, Reynolds numbers, and experimental rates. As mentioned previously, these correction factors were not experimentally determined for the first five oxidation runs. Empirical relations were found by least squares curve-fitting the values that were determined experimentally. These equations are

$$C_D = 1.00233 + 1.1522 \times 10^{-4}Re - 1.8348 \times 10^{-7}Re^2 \qquad (42)$$

and

$$C_R = 0.89318 - 2.0005 \times 10^{-4}Re - 3.6245 \times 10^{-14}Re^z \qquad (43)$$

where $z = T_f/T_a$. From these equations values for the correction factors were calculated and applied to the data for the first five runs.

As discussed in Chapter IV, the experimental scatter is difficult to evaluate because the oxidation rate depends on the wire diameter and the wire diameter was not held constant throughout the study. The data of this forced convection study are not numerous enough to calculate the approximate experimental scatter by the method used by Kraus [11]. However, the data for the low Reynolds number region were obrained on a similar apparatus as the natural convection study and the overall correlation disparity of 7.76 percent reported in Table 5 compares favorably with the approximate experimental scatter of 8.8 percent for the naturally convected study. The correlation disparity at high Reynolds numbers has been stated as 21.44 percent, overall. This implies the anticipated increase in experimental scatter. The experimental scatter was expected to be greater at the high Reynolds numbers because the experimental conditions were not as easily controlled. At high Reynolds numbers the oxidation rates became fast enough that the temperature of the wire was difficult to maintain at a

constant value. It is estimated that the experimental scatter for this portion of the study would be about one and one half times greater than those experiments performed in the oxidation cell.

CHAPTER VII

SUMMARY

The oxidation rate of iridium was assumed to be controlled by the diffusion of the oxide species through the boundary layer at high pressures and by the evaporation of the oxide species from the metal surface at low pressures. After surveying the previous work concerning iridium oxides the important species were concluded to be Ir(g), IrO_2(g), and IrO_3(g). On this basis a theoretical model was proposed and an equation formulated to predict the rate of surface recession of iridium wires oxidized at high temperatures throughout a wide range of pressures.

Experimental data of other researchers were corrected and further experimental work performed so that data were available for a wide range of conditions. It was found that the calculated results from the theoretical model correlated quite well with the experimental results. The major problem which was encountered in using the theoretical equation was to determine the convective heat transfer coefficient for the wire so that the mass transfer coefficient could be calculated. In the case of natural convection this was accomplished by experimentally supplementing a general form from the literature by a function derived specifically for the oxidation cell. For the forced convection study an equation was found in the literature which dealt with wires at high temperatures but the problem became one of circumferentially averaging the parameters since the

local value of the quantities varied around the circumference of the wire.

APPENDIX A

TABLE 6

Experimental Data for Naturally Convected Oxidation in Pure Oxygen

Run No.	Wire Temp. (°C)	Press. (Torr)	Wire Diam. (cm)	Experimental Rate (cm/sec)	Calculated Rate (cm/sec)
1*	1675	1.0E 00	0.0396	3.41E-07	2.43E-07
2*			0.0591	2.36E-07	2.00E-07
3*			0.0477	2.42E-07	2.23E-07
4*			0.0507	2.60E-07	2.16E-07
5*		1.0E 01	0.0597	5.52E-07	5.14E-07
6*			0.0620	5.18E-07	5.00E-07
7*			0.0450	6.09E-07	6.33E-07
8*			0.0482	6.37E-07	6.02E-07
9*		1.0E 02	0.0564	1.41E-06	1.49E-06
10*			0.0595	1.45E-06	1.44E-06
11*			0.0493	1.53E-06	1.64E-06
12*			0.0459	1.55E-06	1.72E-06
13*		1.0E 03	0.0506	6.14E-06	7.00E-06
14*			0.0596	5.70E-06	6.50E-06
15*			0.0549	6.31E-06	6.74E-06
16*			0.0500	7.05E-06	7.05E-06
17*			0.0448	7.89E-06	7.44E-06
18*			0.0388	9.09E-06	8.04E-06
19*			0.0556	7.59E-06	6.70E-06
20*			0.0490	6.85E-06	7.14E-06
21*	1820	1.0E 00	0.0474	4.32E-07	4.83E-07
22*			0.0497	4.05E-07	4.73E-07
23*			0.0442	4.73E-07	5.00E-07
24*		5.0E 01	0.0581	1.71E-06	1.68E-06
25*			0.0626	1.51E-06	1.59E-06
26*			0.0437	2.16E-06	2.07E-06
27*		1.0E 03	0.0408	9.12E-06	9.52E-06
28*			0.0443	8.89E-06	9.12E-06
29*			0.0471	9.63E-06	8.81E-06
30*	1965	7.5EE-05	0.0583	9.06E-09	1.09E-08
31+			0.0493	1.20E-08	1.09E-08
32+			0.0556	1.12E-08	1.09E-08
33+		5.0E-04	0.0453	1.58E-08	1.15E-08
34*			0.0590	1.07E-08	1.15E-08
35*			0.0545	1.06E-08	1.15E-08
36+		1.0E-02	0.0489	3.08E-08	2.40E-08
37+			0.0470	3.05E-08	2.40E-08

TABLE 6 (Cont.)

Run No.	Wire Temp. (°C)	Press. (Torr)	Wire Diam. (cm)	Experimental Rate (cm/sec)	Calculated Rate (cm/sec)
38+	1965	1.0E-02	0.0490	3.37E-08	2.40E-08
39+		5.0E-02	0.0471	6.43E-08	7.52E-08
40*			0.0591	9.38E-08	7.45E-08
41*			0.0624	7.40E-08	7.43E-08
42+		1.0E-01	0.0494	1.43E-07	1.35E-07
43*			0.0515	1.46E-07	1.34E-07
44*			0.0480	1.50E-07	1.35E-07
45*		1.0E 00	0.0458	7.71E-07	7.83E-07
46*			0.0495	5.23E-07	7.59E-07
47*			0.0524	6.51E-07	7.41E-07
48*			0.0483	7.13E-07	7.66E-07
49*			0.0459	7.43E-07	7.83E-07
50*		1.0E 01	0.0435	2.50E-06	2.03E-06
51*			0.0528	2.06E-06	1.77E-06
52*			0.0611	1.55E-06	1.59E-06
53*			0.0574	1.68E-06	1.67E-06
54*			0.0529	1.89E-06	1.77E-06
55*			0.0497	2.04E-06	1.85E-06
56*			0.0468	1.64E-06	1.93E-06
57*			0.0496	2.20E-06	1.85E-06
58*		1.0E 02	0.0389	4.89E-06	4.37E-06
59*			0.0509	3.52E-06	3.60E-06
60*			0.0494	3.42E-06	3.68E-06
61*			0.0468	3.80E-06	3.82E-06
62*		1.0E 03	0.0578	1.02E-05	1.01E-05
63*			0.0607	9.07E-06	9.83E-06
64*			0.0482	1.13E-05	1.10E-05
65*			0.0443	1.22E-05	1.15E-05
66+	2110	7.5E-05	0.0441	4.73E-08	7.52E-08
67+			0.0511	1.04E-07	7.52E-08
68+			0.0451	1.42E-07	7.52E-08
69+		5.0E-04	0.0477	7.61E-08	7.61E-08
70+			0.0570	9.69E-08	7.61E-08
71+			0.0415	1.21E-07	7.61E-08
72+		1.0E-02	0.0491	1.31E-07	9.67E-08
73+			0.0497	1.31E-07	9.67E-08
74+			0.0566	1.29E-07	9.66E-08
75+		5.0E-02	0.0483	2.55E-07	1.81E-07
76+			0.0474	1.21E-07	1.81E-07
77+			0.0597	1.88E-07	1.80E-07

TABLE 6 (Cont.)

Run No.	Wire Temp. (°C)	Press. (Torr)	Wire Diam. (cm)	Experimental Rate (cm/sec)	Calculated Rate (cm/sec)
78+	2110	1.0E-01	0.0476	4.21E-07	2.81E-07
79+			0.0493	2.29E-07	2.80E-07
80+			0.0623	2.14E-07	2.76E-07
81+		1.0E 00	0.0477	1.21E-06	1.42E-06
82+			0.0490	1.05E-06	1.41E-06
83*			0.0557	1.29E-06	1.34E-06
84*			0.0527	1.43E-06	1.34E-06
85*			0.0470	1.16E-06	1.43E-06
86*		5.0E 01	0.0599	4.61E-06	4.54E-06
87*			0.0545	4.88E-06	4.86E-06
88*			0.0492	4.80E-06	5.24E-06
89*		1.0E 03	0.0600	1.24E-05	1.32E-05
90*			0.0561	1.44E-05	1.36E-05
91*			0.0517	1.51E-05	1.50E-05
92+	2260	7.5E-05	0.0562	7.36E-07	4.87E-07
93+			0.0479	6.13E-07	4.87E-07
94*			0.0537	3.30E-07	4.87E-07
95*			0.0618	6.34E-07	4.87E-07
96+		5.0E-04	0.0460	6.47E-07	4.87E-07
97+			0.0610	3.80E-07	4.87E-07
98*			0.0576	4.90E-07	4.87E-07
99*			0.0558	2.53E-07	4.87E-07
100+		1.0E-02	0.0443	8.40E-07	5.07E-07
101+			0.0457	7.97E-07	5.07E-07
102+			0.0592	7.60E-07	5.07E-07
103*		5.0E-02	0.0496	7.43E-07	5.87E-07
104*			0.0503	4.32E-07	5.87E-07
105*			0.0619	7.34E-07	5.83E-07
106*		1.0E-01	0.0544	8.38E-07	6.87E-07
107*			0.0497	6.93E-07	6.82E-07
108*			0.0583	5.04E-07	6.75D-07
109*			0.0499	6.04E-07	6.82E-07
110*		1.0E 00	0.0518	1.42E-06	1.79E-06
111*			0.0534	1.59E-06	1.77E-06
112*			0.0613	1.84E-06	1.69E-06
113*			0.0556	1.74E-06	1.75E-06
114*			0.0458	1.87E-06	1.87E-06
115*			0.0458	2.28E-06	1.87E-06
116*		1.0E 01	0.0537	5.55E-06	4.17E-06
117*			0.0539	5.07E-06	4.16E-06

TABLE 6 (Cont.)

Run No.	Wire Temp. (°C)	Press. (Torr)	Wire Diam. (cm)	Experimental Rate (cm/sec)	Calculated Rate (cm/sec)
118*	2260	1.0E 01	0.0477	5.34E-06	4.53E-06
119*			0.0441	5.99E-06	4.78E-06
120*		1.0E 02	0.0465	1.26E-05	9.35E-06
121*			0.0470	6.51E-06	9.29E-06
122*			0.0568	6.20E-06	8.14E-06
123*			0.0491	8.31E-06	9.01E-06
124*			0.0488	1.03E-05	9.06E-06
125*		1.0E 03	0.0452	3.43E-05	2.78E-05
126*			0.0608	2.09E-05	2.39E-05
127*			0.0474	2.68E-05	2.71E-05
128*			0.0396	3.13E-05	2.99E-05

*Denotes original data gathered by Kraus [11].

+Denotes original data gathered by Wahl [9].

TABLE 7

Experimental Data for Naturally Convected Oxidation in Air

Run No.	Wire Temp. (°C)	Press. (Torr)	Wire Diam. (cm)	Experimental Rate (cm/sec)	Calculate Rate (cm/sec)
1+	1675	5.0E-01	0.0462	3.12E-08	2.86E-08
2+		5.0E 00	0.0500	9.62E-08	7.97E-08
3+			0.0498	7.89E-08	7.99E-08
4+		5.0E 01	0.0496	1.73E-07	1.70E-07
5		2.2E 02	0.0437	3.24E-07	3.54E-07
6			0.0416	3.13E-07	3.65E-07
7+		5.0E 02	0.0480	6.04E-07	5.25E-07
8+			0.0493	5.28E-07	5.18E-07
9	1820	2.2E 02	0.0486	5.69E-07	5.37E-07
10			0.0463	5.65E-07	5.55E-07
11			0.0487	5.19E-07	5.36E-07
12			0.0465	5.39E-07	5.53E-07
13+	1965	7.5E-05	0.0463	1.69E-08	1.10E-08
14+		5.0E-04	0.0489	9.54E-09	1.11E-08
15+		1.0E-02	0.0502	1.33E-08	1.37E-08
16+			0.0487	1.01E-08	1.37E-08
17+		7.5E-02	0.0493	6.71E-08	3.04E-08
18+			0.0467	3.27E-08	3.05E-08
19+		5.0E-01	0.0502	1.06E-07	1.07E-07
20+		5.0E 00	0.0499	3.34E-07	3.02E-07
21+			0.0496	3.27E-07	3.04E-07
22+		5.0E 01	0.0467	5.44E-07	5.62E-07
23+			0.0452	6.57E-07	5.76E-07
24		2.2E 02	0.0426	9.76E-07	9.17E-07
25			0.0399	9.13E-07	9.58E-07
26+		5.0E 02	0.0496	1.20E-06	1.13E-06
27+			0.0496	1.11E-06	1.13E-06
28	2110	2.2E 02	0.0494	1.39E-06	1.49E-06
29			0.0468	1.48E-06	1.54E-06
30			0.0446	1.79E-06	1.59E-06
31			0.0414	1.80E-06	1.67E-06
32+	2260	7.5E-05	0.0465	5.25E-07	5.02E-07
33+			0.0458	8.46E-07	5.02E-07
34+		5.0E-04	0.0466	8.11E-07	5.02E-07
35+			0.0472	6.49E-07	5.02E-07
36+			0.0471	7.74E-07	5.02E-07
37+		1.0E-02	0.0493	7.17E-07	5.04E-07

TABLE 7 (Cont.)

Run No.	Wire Temp. (°C)	Press. (Torr)	Wire Diam. (cm)	Experimental Rate (cm/sec)	Calculate Rate (cm/sec)
38+	2260	7.5E-02	0.0481	8.39E-07	5.17E-07
39+		5.0E-01	0.0476	6.73E-07	5.82E-07
40+			0.0441	6.81E-07	5.91E-07
41+		5.0E 00	0.0556	9.34E-07	7.58E-07
42+			0.0480	9.48E-07	8.32E-07
43+			0.0455	1.01E-06	8.60E-07
44+		5.0E 01	0.0481	1.60E-06	1.34E-06
45+			0.0591	1.27E-06	1.16E-06
46		2.2E 02	0.0490	2.24E-06	2.02E-06
47			0.0463	2.23E-06	2.10E-06
48+		5.0E 02	0.0490	2.82E-06	2.77E-06
49+			0.0606	2.52E-06	2.45E-06

+Denotes original data gathered by Wahl [9].

APPENDIX B

TABLE 8

Experimental Data for Force Convected Oxidation at Low Reynolds Numbers in Pure Oxygen

Run No.	Wire Temp. (°C)	Press. (Torr)	Wire Diam. (cm)	Reynolds No.	Exp. Rate (cm/sec)	Calc. Rate (cm/sec)
1	1675	3.5	0.0496	0.324	6.78E-07	6.81E-07
2		50.	0.0528	0.344	1.48E-06	1.68E-06
3		100	0.0552	0.360	1.96E-06	2.05E-06
4		250	0.0610	0.398	2.47E-06	2.66E-06
5		500	0.0367	0.239	5.33E-06	5.09E-06
6		984	0.0426	0.274	5.93E-06	6.02E-06
7	1820	980	0.0461	0.266	8.47E-06	6.91E-06
8	1965	5.8	0.0406	0.392	3.68E-06	3.45E-06
9		5.7	0.0451	0.432	3.64E-06	3.26E-06
10		10.	0.0608	0.434	2.90E-06	3.08E-06
11		100	0.0328	0.064	5.76E-06	5.49E-06
12			0.0369	0.134	6.22E-06	5.66E-06
13			0.0400	0.260	6.43E-06	6.10E-06
14			0.0608	0.439	4.51E-06	4.64E-06
15			0.0550	0.398	5.14E-06	4.98E-06
16			0.0509	0.368	5.49E-06	5.26E-06
17			0.0445	0.321	6.20E-06	5.80E-06
18			0.0367	0.265	6.86E-06	6.66E-06
19			0.0565	0.445	5.05E-06	5.00E-06
20			0.0465	0.411	5.74E-06	5.92E-06
21			0.0523	0.647	5.91E-06	5.98E-06
22			0.0613	0.976	5.76E-06	5.77E-06
23			0.0603	0.961	5.77E-06	5.83E-06
24		250	0.0381	2.988	1.91E-05	1.58E-05
25		270	0.0545	6.365	1.56E-05	1.49E-05
26		400	0.0441	12.03	2.65E-05	2.56E-05
27		470	0.0294	10.84	4.79E-05	3.82E-05
28		988	0.0502	0.446	1.23E-05	9.50E-06
29		973	0.0425	0.500	1.38E-05	1.15E-05
30	2110	950	0.0535	0.247	1.38E-05	1.05E-05
31	2260	3.5	0.0568	0.209	4.44E-06	5.30E-06
32		50.	0.0598	0.224	1.04E-05	9.25E-06
33		100	0.0402	0.153	1.55E-05	1.40E-05
34		250	0.0461	0.180	1.47E-05	1.52E-05
35		500	0.0514	0.21e	1.65E-05	1.68E-05
36		988	0.0579	0.254	2.00E-05	1.88E-05

NOTE: Original data gathered by Tempero [25].

TABLE 9

Experimental Data for Force Convected Oxidation at High Reynolds Numbers

Run No.	Wire Temp. (°C)	Wire Diam. (cm)	C_D	Reynolds No.	C_R	Exp. Rate (cm/sec)	Calc. Rate (cm/sec)
1	1675	0.0450	1.010*	81.36	0.877+	4.44E-06	4.23E-06
2		0.0202	1.010*	76.98	0.878+	4.57E-06	4.42E-06
3	2260	0.0412	1.005*	26.02	0.888+	1.52E-05	1.64E-05
4		0.0361	1.005*	22.98	0.889+	1.66E-05	1.77E-05
5	1675	0.0629	1.006*	600.6	0.772+	5.96E-06	7.58E-06
6		0.0616	1.008	575.7	0.766	7.17E-06	7.56E-06
7	2260	0.0535	1.020	356.8	0.689	2.77E-05	4.00E-05
8		0.0511	1.020	334.7	0.845	2.95E-05	4.05E-05
9	1965	0.0459	1.025	139.5	0.628	7.93E-06	1.17E-05
10		0.0478	1.003	141.1	0.996	6.38E-06	1.13E-05
11		0.0460	1.016	138.5	0.954	9.14E-05	1.17E-05
12°	1820	0.0400	1.024	67.57	0.828	4.72E-05	4.88E-05
13°		0.0489	1.010	79.93	0.794	3.84E-05	4.28E-05

*Calculated by Eq. (42)

+Calculated by Eq. (43)

°These two runs performed in oxygen, all others in air.

REFERENCES

1. R.T. Wimber, High-Temperature Oxidation of Iridium, First Annual Progress Report, RLO-2228-T1-1, February, 1971.

2. E.H.P. Cordfunke and G. Meyer, "The System Iridium-Oxygen, I. Measurements of the Volatile Oxide of Iridium", Rec. Trav. Chim., 81, pp. 495-504, 1962.

3. C.B. Alcock and G.W. Hooper, "Thermodynamics of the Gaseous Oxides of the Platinum-Group Metals", Royal Society of London, Proceeding Series A, 254, pp. 551-61, 1960.

4. N.H. Schafer and H.J. Heitland, "Gleichgewichtsmessungen im System Iridium-Sauerstoff Gasformiges Iridiumtroxyd", Z. Anorg. Allgem.Chem., 304, pp. 249-65, 1960.

5. L. Holburn, et al, Wiss.Abh.Physik-Techn.Reichsanst., 4, p. 85, 1904. Summarized in Ref. 4.

6. J.H. Norman, et al, "Mass Spectrometric Study of Gaseous Oxides of Iridium", Journal of Physical Chemistry, 42, pp. 1123-4, 1965.

7. A. Olivei, "Methods for Studying Oxygen-Platinum Metals Interaction", Journal of the Less Common Metals, 29, pp. 11-23, 1972.

8. R.T. Wimber and H.G. Kraus, "Oxidation of Iridium", Metallurgical Transactions, 5, pp. 1565-72, 1974.

9. N.K. Wahl, Natural-Convective High-Temperature Oxidation of Iridium, Master's Thesis, Montana State University, June, 1974.

10. R.T. Wimber, High Temperature Oxidation of Iridium, Third Annual Progress Report, RLO-2228-T1-5, February, 1973.

11. H.G. Kraus, Natural Convection, High Temperature Oxidation of Iridium, Master's Thesis, Montana State University, June, 1973.

12. A.W. Searcy, D.V. Ragone, and U. Colombo, Chemical and Mechanical Behavior of Inorganic Materials, pp. 108-110, Wiley-Interscience, New York, 1970.

13. T.K. Sherwood and R.L. Pigford, Absorption and Extraction, 2nd ed., pp. 52-92, McGraw-Hill, N.Y., 1952.

14. J.J. Halvorson and R.T. Wimber, J. Appl. Phys., 43, pp. 2519-22, 1972.

15. J.R. Welty, C.E. Wicks, and R.E. Wilson, Fundamentals of Momentum, Heat, and Mass Transfer, p. 551, J. Wiley and Sons, New York, 1969.

16. A.J. Madden, Jr. and E.L. Piret, Proceedings of the General Discussion on Heat Transfer, pp. 328-33, IME and ASME, New York, 1951.

17. Y. Aihara and H. Koyama, AIAA Journal, 10, pp. 1386-87, 1972.

18. R.T. Wimber and J.J. Halvorson, J. Mater., 7, pp. 564-67, 1972.

19. R.E. Emmert and R.L. Pigford, Chemical Engineers Handbook, 4th ed., Sect. 14, pp. 20-21, McGraw-Hill, New York, 1963.

20. R. Honig and D.A. Kramer, Techniques of Metals Research, Vol IV, Part I, pp. 515-16, John Wiley and Sons, New York, 1970.

21. J. Hilsenrath, et al, Tables of Thermal Properties of Gases, NBS Circ. 564, 1955.

22. E.H.P. Cordfunke and G. Meyer, op. cit., pp. 670-78.

23. W.E. Bell, M. Tagami, and R.E. Inyard, J. Phys. Chem., 70, pp. 2048-50, 1966.

24. L. Brewer, Chem. Revws., 52, pp. 1-75, 1953.

25. C.R. Tempero, The High Temperature Oxidation of Iridium in a Forced Convection Oxygen Atmosphere, Master's Thesis, Montana State University, June, 1972.

26. R. Hilpert, Forsch. Gebrete Ingenieurw., 4, pp. 215-24, 1933.

27. R.M. Fand and K.K. Keswani, Int. J. Heat Mass Transfer, 15, pp. 559-62, 1972.